Lab on a Chip

3D printed microfluidic devices for lipid bilayer recordings

Journal:	*Lab on a Chip*
Manuscript ID	LC-ART-11-2021-001077.R1
Article Type:	Paper
Date Submitted by the Author:	24-Jan-2022
Complete List of Authors:	Ogishi, Kazuto; The University of Tokyo Graduate School of Information Science and Technology, Osaki, Toshihisa; Kanagawa Institute of Industrial Science and Technology, Artificial Cell Membrane Systems Group; The University of Tokyo, Institute of Industrial Science Morimoto, Yuya; The University of Tokyo, Graduate School of Information Science and Technology Takeuchi, Shoji; The University of Tokyo, Graduate School of Information Science and Technology; Kanagawa Institute of Industrial Science and Technology, Artificial Cell Membrane Systems Group; The University of Tokyo, Institute of Industrial Science

ARTICLE

3D printed microfluidic devices for lipid bilayer recordings

Kazuto Ogishi [a], Toshihisa Osaki [bc], Yuya Morimoto [a] and Shoji Takeuchi [abc*]

Received 00th January 20xx,
Accepted 00th January 20xx

DOI: 10.1039/x0xx00000x

This paper verifies the single-step and monolithic fabrication of 3D structural lipid bilayer devices using stereolithography. Lipid bilayer devices are utilized to host membrane proteins in vitro for biological assays or sensing applications. There is a growing demand to fabricate functional lipid bilayer devices with a short lead-time, and the monolithic fabrication of components by 3D printing is highly anticipated. However, the prerequisites of 3D printing materials which lead to reproducible lipid bilayer formation are still unknown. Here, we examined the feasibility of membrane protein measurement using lipid bilayer devices fabricated by stereolithography. The 3D printing materials were characterized and the surface smoothness and hydrophobicity were found to be the relevant factors for successful lipid bilayer formation. The devices were comparable to the ones fabricated by conventional procedures in terms of measurement performances like the amplitude of noise and the waiting time for lipid bilayer formation. We further demonstrated the extendibility of the technology for the functionalization of devices, such as incorporating microfluidic channels for solution exchangeability and arraying multiple chambers for robust measurement.

Introduction

Membrane proteins, which are relevant to signal transduction and substance transport across cell membranes, have attracted a great deal of attention in the research fields of drug discovery[1]. In recent years, membrane proteins have also been used as chemical sensors due to their high specificity and sensitivity to their ligand molecules[2]. Several devices have been developed for the formation of a lipid bilayer that is required for the use of membrane proteins in vitro, by using microfluidic technology like microchannels and/or microwells to control water-oil interfaces where the bilayer is formed[3–5]. For example, in the droplet contact method (DCM)[6–8], a lipid bilayer is spontaneously formed at the interface of two droplets, simply by infusing aqueous solutions in lipid-dispersed oil[9]. A typical DCM device consists of a double-well (DW) chamber, which is a chamber with two cylindrical wells overlapping each other, and a perforated separator to reduce the contact area for stabilizing the bilayer. A pair of electrodes and an amplifier are connected for the electrical monitoring of membrane proteins (Fig. 1a). These devices have already been used to measure the properties of membrane proteins including transporters[10], ion channels[8,11], and nanopores[12,13].

With the rapid development of 3D printing technology, it is now becoming possible to produce 3D structural microdevices without conventional MEMS procedures[14–16]. Fabrication of lipid bilayer devices has also been reported using 3D printed components[17,18], and the technology will contribute to the rapid prototyping of functional lipid bilayer devices, because the current fabrication process requires laborious procedures including micromachining and manual assembly (Fig. 1b). However, the requisite characteristics of 3D printed devices for successful lipid bilayer formation have not yet been clarified, especially concerning the materials and principles of 3D printers.

In this study, we examine the feasibility of applying stereolithographic technology for the fabrication of lipid bilayer devices and the measurement of membrane proteins (Fig. 1c). First, we verify the success rates of lipid bilayer formation on DCM devices fabricated by 3D printers with different printing principles and materials. The bilayer formation is confirmed by the incorporation of nanopore-forming membrane proteins into the bilayer. Then, we demonstrate that the devices are comparable to the ones made by conventional fabrication methods, in terms of the amplitude of electrical noise and the waiting time for lipid bilayer formation. We further evaluate the extendibility of the technology by integrating microfluidic channels for solution exchangeability and by arraying DW chambers for simultaneous electrical recordings of membrane proteins on multiple lipid bilayers.

Experimental

Materials and reagents

Three combinations of 3D printers with resins were used to fabricate the DCM devices: microArch™ S140 and HTL resin (microArch) (BMF, U.S.A.), DigitalWax® 028J and THERMA DM 210 resin (DigitalWax) (DWS, Italy), and AGILISTA-3110 and AR-M2 resin (AGILISTA) (Keyence, Japan). Three surface coatings were compared on the 3D printed devices: Novec™ 1700

[a] Graduate School of Information Science and Technology, The University of Tokyo, 7-3-1 Hongo, Bunkyo-ku, Tokyo, 113-8656, JAPAN.
[b] Kanagawa Institute of Industrial Science and Technology, 3-2-1 Sakado, Takatsu-ku, Kawasaki, Kanagawa, 213-0012, JAPAN.
[c] Institute of Industrial Science, The University of Tokyo, 4-6-1 Komaba, Meguro-ku, Tokyo, 153-8505, JAPAN.
* Corresponding author. E-mail: takeuchi@hybrid.t.u-tokyo.ac.jp

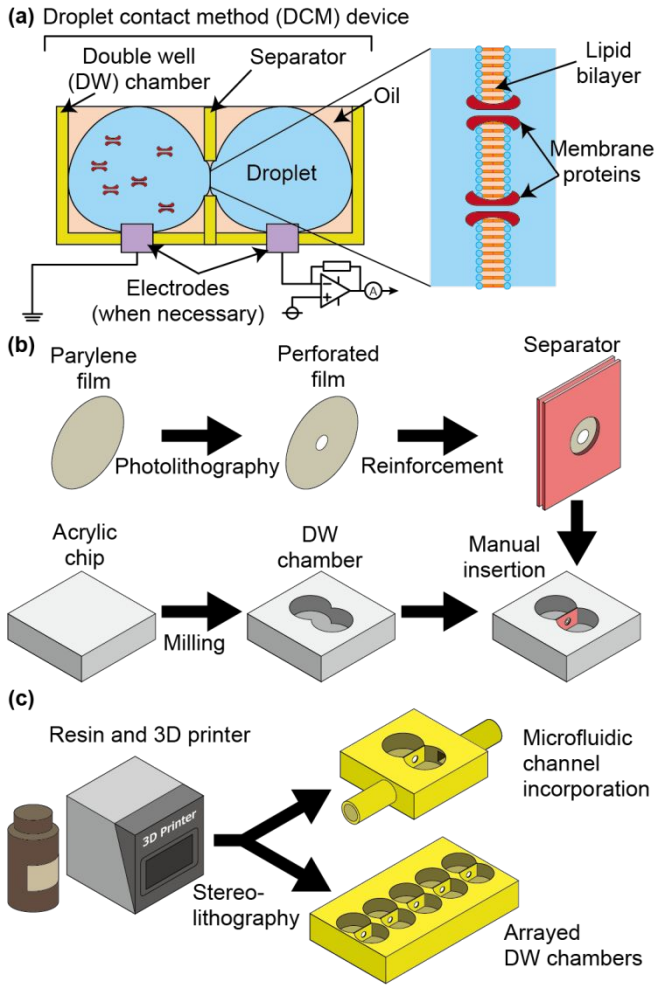

Figure 1: (a) A schematic diagram of a DCM device. Two droplets in a DW chamber contact at the microaperture on a separator, forming a lipid bilayer. (b) Conventional fabrication procedure of a DCM device. The device components were individually fabricated and assembled manually. (c) Fabrication procedure of a DCM device by stereolithography. The components can be monolithically fabricated with a single process.

(Novec) (3M Japan, Japan), Parylene C (Parylene) (Specialty Coating Systems, U.S.A.), and 2-methacryloyloxyethyl phosphorylcholine (MPC) polymer LIPIDURE® CR3001 (MPC) (NOF, Japan). Silver/silver chloride (Ag/AgCl) ink (BAS, Japan), silver rods (Tanaka kikinzoku, Japan), and pin headers (Useconn Electronics, Taiwan) were utilized as electrode materials for electrical monitoring with the devices. An in-house developed amplifier and measurement software (PocketAmp U2)[19] were used for the electrical measurement of transmembrane current caused by membrane proteins. A multiplexer TC4051BP (Toshiba, Japan) was used for simultaneous electrical recordings of multiple lipid bilayers.

As a reagent for the lipid bilayer formation, 1,2-diphytanoyl-sn-glycero-3-phosphocholine (DPhPC) was purchased from Avanti Polar Lipids (U.S.A.). Nanopore-forming membrane protein α-hemolysin (αHL) from Staphylococcus aureus and *n*-decane were purchased from Sigma-Aldrich (U.S.A.). Other reagents for a buffer solution were obtained from FUJIFILM Wako Pure Chemical (Japan) and dissolved in ultrapure water (collected from Direct-Q UV 3, Merck Millipore, U.S.A.). Calcein, a green fluorescent dye, was used for fluorescence observation (Sigma-Aldrich, U.S.A.). All reagents were used without further purification.

Monolithic fabrication of the DCM devices by 3D printers

Fig. 2 shows the images of three DCM devices examined in this study. Three designs were used for the characterization of the 3D printed DCM devices: a single DW chamber (Fig. 2a), a DW chamber with a pair of microfluidic channels for solution exchange (Fig. 2b), and a device containing five DW chambers in a row (Fig. 2c). The wells of the DW chamber were 2.2 or 4 mm in diameter and 3 mm in depth, with holes at the bottom or the sidewall of wells for the subsequent formation of Ag/AgCl electrodes. The separator had a thickness (*W*) of 40, 80, or 200 µm and an aperture diameter (*D*) of 400, 800, 1200, or 1600 µm. For the solution exchange device, the microfluidic channels were connected to only one of the wells of the DW chamber. The well to which the channels were connected and where the solution was exchanged is denoted as "Well A" and the opposite well as "Well B". The cross-section of the microchannels was square, whose length of a side was 500 µm. The channels were connected to the tubing outside the chip via connectors. For the DW chamber array, the distance between each chamber was set at 2.54 mm, which was the standard pitch of a pin header on a circuit board.

The DCM devices were monolithically fabricated using the three 3D printers with different printing principles: digital light processing for microArch, laser stereolithography for DigitalWax, and material jetting for AGILISTA. All devices were designed using CAD software (Autodesk Inventor® 2019 Professional) and were printed using the respective 3D printers. The printed devices were then cleaned with ethanol and thoroughly dried with air blow.

The surfaces of the printed DCM devices were modified with the three chemicals; with Novec and MPC, the surfaces were coated simply by dipping into the coating solution, slowly pulling up, and drying. Parylene was applied by vapor deposition using a parylene coater, LABCOTER PDS2010 (Specialty Coating Systems, U.S.A.), to achieve a film thickness of 2 µm.

Electrodes were embedded in the DCM devices. Silver rods or pin headers were first inserted into holes in the wells or sidewall of the DW chambers. Ag/AgCl ink was then carefully applied to fill in the gap between the holes and the electrodes to suppress leakage of solutions. After the ink was solidified, Ag/AgCl surface was formed.

Characterization of the 3D printing materials

To examine the relationship between a successful lipid bilayer formation and the principles of the 3D printer, resins, and surface coatings, we first measured the printing accuracy, the surface roughness of the separator, and the contact angle of the device to water and oil.

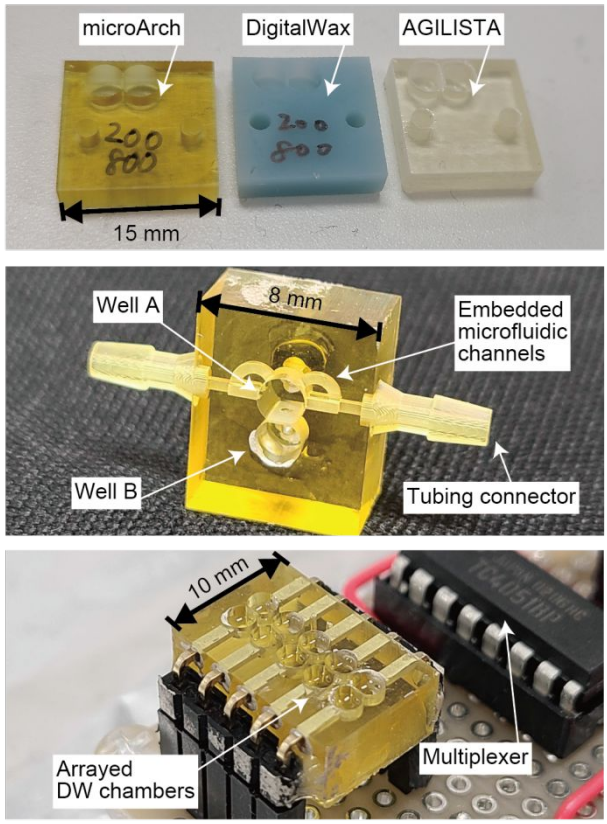

Figure 2: Images of the fabricated DCM devices. (a) The DCM device for the characterization of 3D printing materials and devices. The device consists of a single DW chamber. (b) The DCM device for the solution exchange. The device contained embedded microfluidic channels for exchanging a solution in one of the wells. (c) The DCM device for the simultaneous electrical recording. The device consists of five DW chambers in a row. The pairs of electrodes were connected to each DW chamber for electrical recordings. The connection of the electrodes to a single amplifier was switched with a multiplexer.

The printing accuracy was evaluated by comparing the CAD designs and the printed objects[20]. A separator was designed with a thickness of 200 µm, fabricated with each printer, and the actual thickness was measured with a laser microscope (VK-X210, Keyence, Japan). The deviation of the thickness between the design and printed object was then calculated.

The surface roughness was calculated by the arithmetic average roughness (R_a) of a surface profile, which was obtained with a stylus profilometer (Dektak 6M, BRUKER, U.S.A.) by tracing the surface with a microneedle from the bottom of the separator for the length of 2 mm to the stacking direction.

The contact angle was measured by pipetting a 1-µL droplet of ultrapure water or *n*-decane on the fabricated device. An image of the droplet was taken from the side with a microscope (VM-900, Keyence, Japan) and contact angles were then calculated based on the height-width method with ImageJ.

Lipid bilayer formation and αHL nanopore incorporation

The formation of a lipid bilayer by DCM and the incorporation of membrane proteins were achieved in the same way as the previous studies[7,8]. First, lipid-dispersed oil (10 mg/mL DPhPC in *n*-decane) was pipetted into each well of the DW chamber. Then, KCl buffer solution (1.0 M with 10 mM phosphate buffer adjusted at pH 7.0) which contained αHL monomers was infused into the oil in each well. A lipid monolayer was formed at the interface between the oil and an aqueous droplet of KCl solution. At the aperture of the separator, the monolayers of two droplets came into contact and the lipid bilayer was formed[8]. αHL monomers bound to the lipid bilayer and formed a nanopore as a heptamer[21].

The volume of each solution was determined according to the design of the device. Specifically, for the devices depicted in Fig. 2a, 3 µL of the lipid-dispersed oil and 21 µL of the KCl buffer solution were introduced into each well of the DW chamber, and for the devices depicted in Fig. 2b and 2c, the oil was 1 µL and the KCl solution was 7 µL since the wells were smaller than those of the devices in Fig. 2a.

The fabricated DW chambers were repeatedly used at least three times after several minutes of ultrasonic cleaning in ethanol to flush out lipids. Device deterioration, such as the peeling of the surface coatings or the Ag/AgCl ink, was not observed after cleaning.

Ionic current recording of the incorporated αHL nanopores

The electrical recordings with the DCM devices were conducted by connecting the device to the electrical amplifier through printed circuit boards or a BNC connector. The in-house developed amplifier PocketAmp U2 was a trans-impedance amplifier with the gain of 1 GΩ. The ionic current was measured under a bias voltage of 10-50 mV. The current data was with a 5 kHz sampling frequency and applied an analog low-pass filter with a cutoff frequency of 1 kHz. The measurements were carried out in a Faraday cage to prevent electromagnetic noise. The recorded data were visualized and analyzed with Clampfit 11.1 (Molecular Devices, U.S.A.).

The simultaneous measurement of multiple lipid bilayers was achieved by switching the chamber with a multiplexer; the chambers were scanned in sequence every 0.2 s by the control from Arduino Uno (Arduino Holding, Italy). To reduce the electrical noise which was from a commercial power supply, the Arduino and multiplexer were driven by a 9V battery, not by a socket. The obtained data were split into separate current signals from each chamber using Excel VBA. A transient current originated from the capacitance of a lipid bilayer[22] was observed with switching the multiplexer. Therefore, the current value of each chamber was chosen after the transient current had become constant.

Characterization of the 3D printed DCM devices

The performance of the 3D printed DCM device was characterized based on the success rate of the lipid bilayer formation, the amplitude of electrical noise, and the waiting time for lipid bilayer formation.

The successful lipid bilayer formation was approved by observing the nanopore incorporation after the manipulation of bilayer formation. The two aqueous droplets in the DW chamber, which contact at the aperture of the separator, were

manually separated by tracing the aperture surface with a hydrophobic plastic stick. This manipulation is called re-painting[23]. We fused the droplets on purpose and conducted re-painting to derive the success rate using the following equation.

$$(Success\ rate\ of\ the\ lipid\ bilayer\ formation) = \frac{(No.\ of\ successful\ bilayer\ formation)}{(No.\ of\ total\ \text{re-painting})}$$

The amplitude of electrical noise (root mean square (rms) noise) was defined as the standard deviation of the current data just before the incorporation of αHL nanopores.

The waiting time for lipid bilayer formation was defined as the duration between the re-painting manipulation and the incorporation of the first αHL nanopore, based on the ionic current recording.

Solution exchange with embedded microfluidic channels

The solution exchange experiment was performed using the DCM devices incorporated with microfluidic channels. Two syringe pumps (LEGATO® 180, KD Scientific, U.S.A.) were connected to the connectors of the DCM device via silicone tubing for delivery and suction of the solution. The flow rate of each pump was set at 1 µL/s. To reduce electromagnetic noise during measurement, the tubing was wrapped with aluminum foil and grounded.

To verify the solution exchange, the fluorescence intensity of the droplet in each well of the DW chamber was measured. The KCl buffer solution containing 100 µM calcein and 1 nM αHL, was used for the formation of a lipid bilayer and exchanged to the KCl solution without calcein by the pumps. The time-series change in the intensity was observed with a fluorescence microscope (MVX10, OLYMPUS, Japan) by capturing time-lapse images at 8 fps. The images were then analyzed by ImageJ, an image processing software (NIH, U.S.A.). The electrical measurement was simultaneously performed to confirm that the lipid bilayer was properly formed and not ruptured during the solution exchange.

Results and discussion

Characteristics of the 3D printing materials

To determine the requisite characteristics of the printing materials for the devices achieving successful lipid bilayer formation, we first measured the printing accuracy, the surface roughness, and the surface wettability for each combination of 3D printers and surface coating agents. As shown in Fig. 3 and Table 1, the characteristics depended on the printers and coating agents used. As for the printing accuracy, the microArch printer presented the most accurate thickness of the separator, while the AGILISTA printer was the worst (Fig. 3b). In a previous study, it was suggested that the material jetting method, which was used in AGILISTA, produced relatively large deviations when printing thin walls[24,25], and the present result showed a similar trend. Regarding the surface roughness, both the microArch and DigitalWax printers showed better surface smoothness than the AGILISTA printer (Fig. 3c). This result was

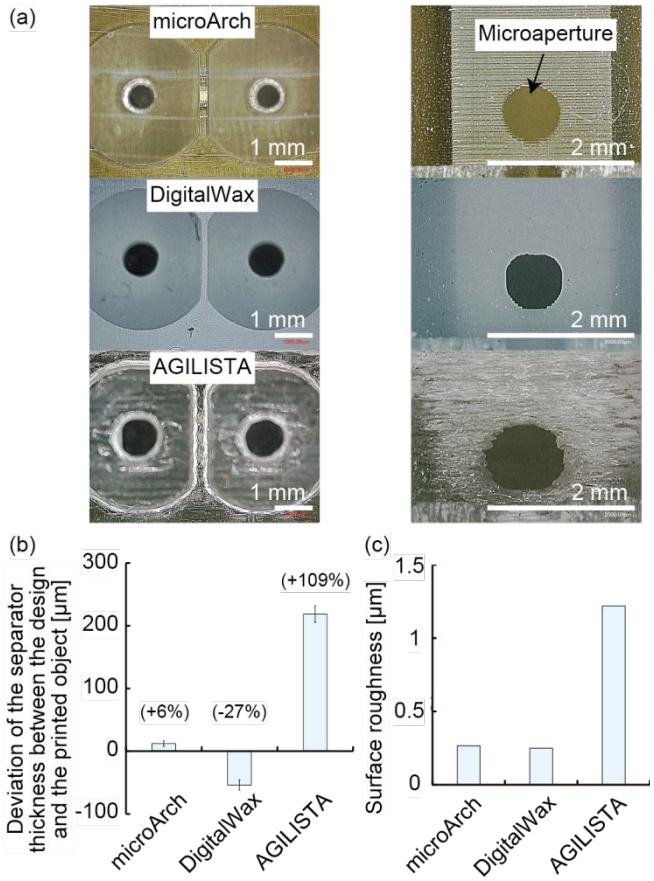

Figure 3: Characterization of the 3D printing materials in terms of the printing accuracy and surface roughness for each 3D printer. (a) Top and front views of the separators made by 3D printers. (b) Deviation of the separator thickness between the design (200 µm) and the printed object (n = 9). Values in parentheses show ratios of the deviations to the designed value. Error bars represent standard deviation. (c) Surface roughness of the separator (n = 2).

Table 1: Characterization of the 3D printing materials in terms of surface wettability (Contact angles with ultrapure water and n-decane).

Printer	Coating	θ_{water} (°)	$\theta_{n\text{-decane}}$ (°)
microArch	-	28 ± 6	< 10
	Novec	78 ± 1	36 ± 5
	Parylene	86 ± 4	< 10
	MPC	20 ± 3	< 10
DigitalWax	-	64 ± 12	< 10
	Novec	103 ± 2	49 ± 2
	Parylene	93 ± 6	< 10
	MPC	35 ± 4	< 10
AGILISTA	-	32 ± 3	< 10
	Novec	96 ± 9	53 ± 5
	Parylene	88 ± 0	< 10
	MPC	34 ± 12	< 10

θ_{water} represents water contact angle.
$\theta_{n\text{-decane}}$ represents *n*-decane contact angle.
Average ± standard deviation (n = 3).

also supported by the previous studies, indicating that 3D printing technology utilizing laser beams, including stereolithography used in DigitalWax and digital light processing used in microArch, produced a smooth and homogeneous surface[20,24].

The surface wettability depended on the resins used for the printers. As shown in Table 1, resins of the microArch and AGILISTA printers, both of which were based on acrylic polymer, were hydrophilic, while that of the DigitalWax printer, which consists of ceramic resin, was hydrophobic. We adjusted the wettability by three coatings. The fluorinated coating of Novec made the object surfaces to be hydrophobic and moderately oleophobic. Parylene coating provided hydrophobic but oleophilic surfaces. MPC coating showed hydrophilicity and oleophilicity on the surfaces.

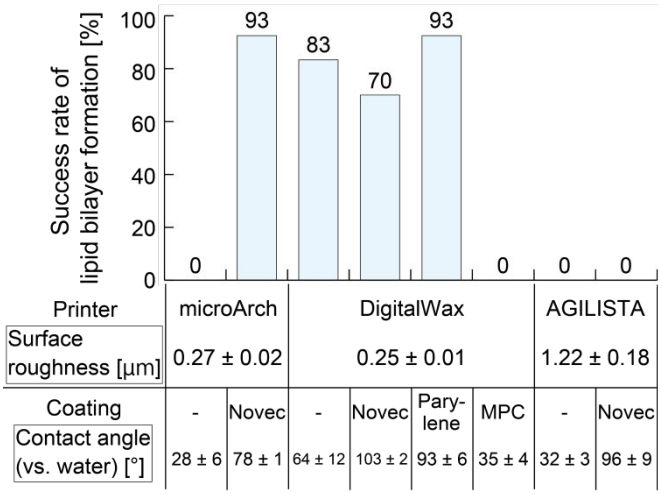

Figure 4: Characterization of the 3D printed DCM devices from the viewpoint of the success rate of lipid bilayer formation (W = 200 μm, D = 800 μm) (n > 14). Lipid bilayer formation was confirmed by the electrical signal caused by incorporation of αHL nanopore (concentration: 100 nM). The specific values for surface roughness and contact angle were taken from Fig. 3 and Table 1.

Lipid bilayer formation with the 3D printed DCM devices

To clarify the favorable characteristics of 3D printed devices for reproducible lipid bilayer formation, we examined the success rate of the bilayer formation for each combination of the printing materials and coatings. As shown in Fig. 4, the success rate was strongly dependent on the physical properties of devices, especially hydrophobicity and surface roughness.

Regarding hydrophobicity, previous works also applied a hydrophobic separator to successfully form a lipid bilayer[26]. Since hydrophobic surfaces in air are oleophilic in water[27], the hydrophobic separator will be covered with oil in aqueous solutions after the reagents are loaded to the DCM devices. In this context, a hydrophobic surface allows the separator to keep aqueous solution separate by oil at the aperture and to facilitate the orientation of lipid molecules on the surface, both of which are inevitable for forming a lipid bilayer. In Fig. 4, the DCM devices fabricated by microArch or DigitalWax succeeded in forming a lipid bilayer when the device surfaces were hydrophobic, suggesting the results were in line with the previous ones[26,27].

In contrast, the device fabricated by AGILISTA showed a different trend. Lipid bilayer formation failed even though the surface of the device was hydrophobic with the Novec coating. Specifically, the droplets were not separated even after the re-painting manipulation. This result was probably attributed to the surface roughness of the device. As shown in Fig. 3c and Fig.S1, the separator fabricated by AGILISTA had a relatively rough surface. We consider that this roughness disturbed bilayer formation probably because the lipid-dispersed oil was ejected from the aperture, guided through the rough surface.

The present results indicated that the process of lipid bilayer formation may be strongly influenced by the micrometer-order structures of the separator surfaces. In the discussion above, the negative effect of the rapid oil expulsion from apertures was considered, but it would also be possible that the rapid oil ejection facilitates successful lipid bilayer formation if surface structures are carefully designed. Several works, in fact, demonstrated surface structures to make lipid bilayer processes more stable[28–30]. We therefore believe the differences in the separators investigated in this study, especially in terms of surface roughness and hydrophobicity, would give an insight into controlling the lipid bilayer formation process in DCM devices more precisely, even with the separators fabricated by methods other than 3D printing, such as acrylic machining[22] or photolithography[29,31].

When the separator met the above-mentioned conditions of high hydrophobicity and low surface roughness, the success rate of lipid bilayer formation reached 70-93%. In a previous study, the success rate ranged from 47% to 86%[26], and our 3D printed device achieved a similarly good success rate.

Performance of the 3D printed DCM devices

To demonstrate that the 3D printed DCM devices, fabricated with properly selected materials, are comparable to the ones fabricated manually in the previous works, we examined the performance of the devices in terms of the amplitude of electrical noise and the waiting time for lipid bilayer formation (Fig. 5).

The electrical trace of αHL nanopore showed a clear stepwise waveform with an average conductance of 923 pS (Fig. 5a). The conductance was in good agreement with the previous one of a single heptameric nanopore of αHL in 1 M KCl solution, ~ 1 nS[32]. The results indicated that the 3D printed DCM devices were applicable for the formation of a lipid bilayer, incorporation of ion channels, and measurements of transmembrane ionic current attributed to the ion channels.

Next, we evaluated the amplitude of electrical noise of ionic current through the formed lipid bilayer. As shown in Fig. 5b, the smaller the aperture diameter *D* of the separator (the images are shown in Fig. S2), the smaller the noise level became. It was considered that the decrease in the aperture diameter *D* led to the decrease in the area of a lipid bilayer, which in turn reduced the electrical noise[33,34]. By contrast, the thickness of separator *W* was not significantly related to the amplitude of

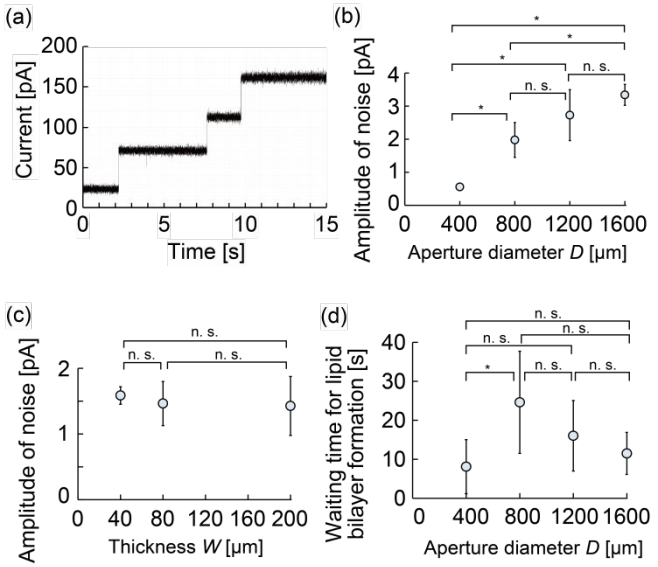

*Figure 5: Performance of the DCM devices made by stereolithography. (a) A representative transmembrane current signal of αHL nanopores (microArch, Novec, W = 200 μm, D = 1200 μm). (b) Relationship between the electrical noise and the aperture diameter D (DigitalWax, Novec, W = 200 μm) (n = 5). (c) Relationship between the electrical noise and the separator thickness W (microArch, Novec, D = 800 μm) (n = 7). (d) Relationship between the waiting time for a lipid bilayer formation and the aperture diameter D (DigitalWax, Novec, W = 200 μm) (n > 10). Error bars represent standard deviation. The significance was assessed by evaluating the pairwise differences among the mean values using Tukey-Kramer test. *p < 0.05, n.s. not significant. Applied voltage: 50 mV. αHL concentration: (a) 10 nM, (b)-(d) 100 nM.*

electrical noise (Fig. 5c), implying that the lipid bilayer area could be independent of the change in the thickness of a separator. Additionally, the combination of device materials was also unrelated to the amplitude of noise (Fig. S3a). It is known that the thicker the separator, the less it affects the electrical noise[33], and we consider the 3D printed separators were thick enough that the materials had almost no effect on the amplitude of noise. These results suggested that, when fabricating DCM devices by stereolithography, a high signal-to-noise ratio of ionic current measurements would be achieved by reducing the aperture diameter, and the separator thickness and materials would be changeable, within the resolution of 3D printers or the conditions about surface roughness and hydrophobicity described in the previous section.

It is known that the large capacitance and small resistance of a planar lipid bilayer impair the current signals of ion channels[35] and suppression of the electrical noise is indispensable to characterize ion channels. In the present study, the RMS electrical noise was suppressed to 0.56 ± 0.10 pA by optimizing dimensions of the separator, which was comparable to previous studies where the RMS noise ranged from 0.4 pA[33] to 0.9 pA[23,26]. Assuming a normal distribution of the current data, the peak-to-peak noise, which determines whether the target signals are resolved by the system, would be 3.3 pA (which is estimated to be 6 times of the RMS noise). A part of ion channels, such as the large-conductance calcium-activated potassium channel (BK)[8,36] or the transient receptor potential vanilloid 4 channel (TRPV4)[37], exhibit conductance over 80 pS, which represents the gating current larger than 4 pA at 50 mV bias. Therefore, the developed devices would likely be able to resolve signals from those ion channels. We consider that more sensitive signal recordings can be achieved by decreasing the aperture diameter, whose applicability would depend on the performance of the 3D printing technology.

The relationship between the waiting time for the lipid bilayer formation and the aperture diameter *D* was shown in Fig. 5d. Lipid bilayers were formed within 40 s regardless of the separator dimensions. Previous work suggested that the waiting time of 50 s was practical enough for repetitive measurements in DCM research[23], and we consider our 3D printed DCM devices also demonstrated sufficient performance in this context.

According to the results above, the optimized 3D printed devices would present the same performance as the previously developed devices[8,23,26,33] and feasible for sensitive and rapid acquisition of ion channel signals.

Solution exchangeability with microfluidic channels

We demonstrated the extendibility of the stereolithographic fabrication of the DCM device. First, microfluidic channels were integrated into the device as shown in Fig. 2b, and the exchangeability of a solution in a DW chamber was verified by fluorescence observation of the chamber and by electrical monitoring of the state of a lipid bilayer. When the solution was pumped into the fabricated device through the microfluidic channels, no leakage or overflow of the solution from the channels or wells was observed, which would be caused by cracking or clogging by improper configuration over the 3D printing process. This result assured the reproducibility of stereolithographic integration of complex structures into the DCM devices.

Time course of the fluorescence intensity of each well is shown in Fig. 6b; The fluorescence images of the wells before and after the solution exchange are shown in Fig. 6c. The initial intensity of each well was normalized to 1. The fluorescence intensity at "well A", to which the microfluidic channels were connected, decreased together with the exchange of the fluorescent solution with aqueous buffer solution. On the other hand, the fluorescence intensity at “well B”, where the solution exchange was not conducted, was almost kept constant. These results indicated that the solution was exchanged by the integrated microfluidic channels without the fusion of the two droplets. Subtracting the background intensity caused by the autofluorescence of the 3D printing materials, the 60-second exchange replaced 88 ± 5% of the solution in the well.

We further confirmed the state of a lipid bilayer over the exchange of the solution using electrical recordings of αHL nanopore incorporation. A representative electrical signal observed over the solution exchange is shown in Fig. 6d. The average value of the stepwise conductance increases was 983

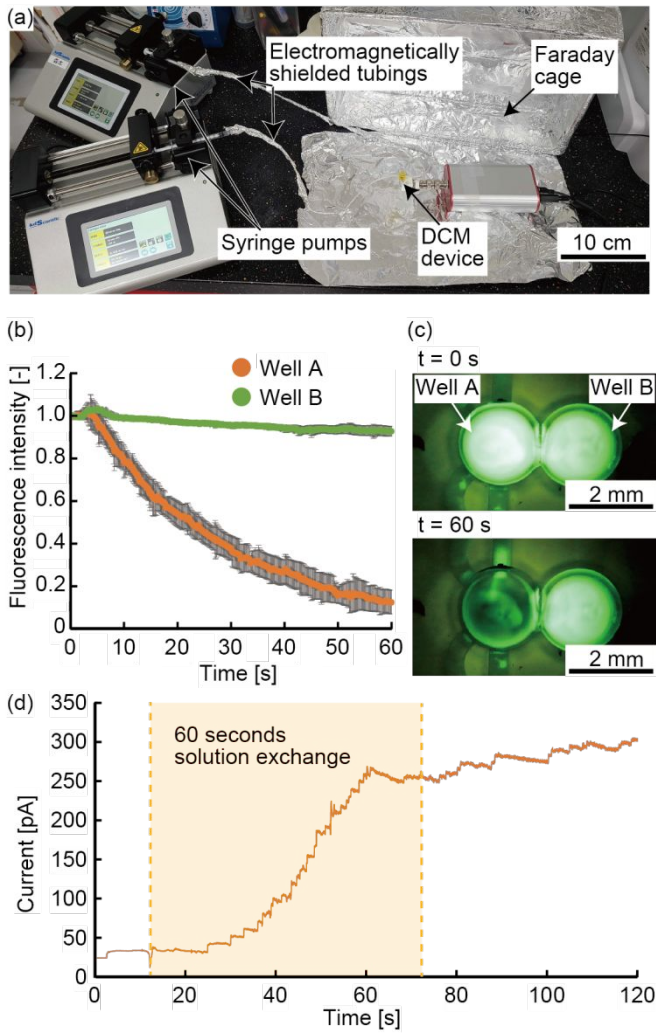

Figure 6: Solution exchange on the DCM device with the integrated microfluidic channels. (a) Setup for electrical measurements for the DCM device together with solution exchange in a well. (b) Time course of the normalized fluorescence intensity of each well over the solution exchange. Error bars represent standard deviation (n = 6). (c) Fluorescent images of the wells on the DCM device at the beginning and end of the solution exchange. (d) A representative transmembrane current signal of αHL nanopores over the solution exchange. The signal was processed by the simple moving average of 40 ms for noise reduction. Applied voltage: 10 mV. Fabrication materials: microArch and Novec. Dimension: W = 80 µm, D = 600 µm. αHL concentration: 1 nM.

pS, which was consistent with the conductance of αHL observed in the device without solution exchange (Fig. 5a), indicating the incorporation of αHL nanopores into the lipid bilayer. Immediately after the first nanopore signal was obtained, which assures the lipid bilayer formation, the solution exchange was started. The continual incorporation of αHL nanopores during the solution exchange confirmed that the bilayer was durable under the pumping pressure for the solution exchange.

With the former technology such as micromilling[11,38], integration of a complex structure with a DCM device was often restricted in its design because of the limitation of the technology. Contrarily, the results suggested that the stereolithographic technology overcame the limitation, simplified the fabrication process in a single step, and enabled the integration of the channels and connectors with the DCM device, which demonstrated solution exchange keeping the bilayer intact.

Simultaneous electrical recordings by arrayed DW chambers

We further verified the extendibility of the stereolithographic fabrication of DCM devices towards the simultaneous electrical recordings of multiple lipid bilayers. An arrayed device consisting of five DW chambers was monolithically fabricated by the microArch printer and Novec coating (Fig. 2c). The lipid bilayers were formed on the device and sequentially monitored with the single amplifier by switching the connections using a multiplexer (Fig. 7a).

A set of ionic current signals recorded with the five DW chambers are shown in Fig. 7b. In this example, lipid bilayers or lipid membranes in chambers 1 and 3 ruptured as time elapsed, resulting in the overflowed currents. In the remaining three chambers, αHL nanopores were incorporated in the formed bilayers, and stepwise current increases like those in Fig. 5a were presented. We confirmed that the average amplitude of electrical noises of those three lipid bilayers was 1.5 ± 0.3 pA, and this noise level, where *D* was 600 µm, was in line with the results in Fig. 5b. Based on these results, we consider that the applied 3D printer demonstrated good reproducibility for fabrication of the DW chambers and separators, which in turn allowed reproducible measurements of ionic current signals of αHL nanopores.

Simultaneous electrical recordings of multiple lipid bilayers are expected to improve the robustness of ion channel analyses or nanopore-based sensing. In the present results, the arrayed DW chambers demonstrated rapid detection of the first αHL nanopore signal, even though the concentration of αHL was set to 0.1 nM, which would require a long detection time, in average, with a single DW chamber[39]. The data availability of the single-molecule measurements with nanopores or ion channels depends on the stochastic protein incorporation into a lipid bilayer. In this study, multiple lipid bilayers on the arrayed chambers increased the probability of protein incorporation, resulting in the rapid signal detection. Since the number of DW chambers can be easily increased using stereolithography, the technology would help the data availability of nanopore or ion channel assays. Additionally, the arrayed DW chambers extended the observation time. As shown in the result, two lipid bilayers remained intact after 3 min of the measurement. Rupture of lipid bilayers has been a major issue for the assays using lipid bilayer devices including DCM[40]. Several studies tackled this issue, by limiting the bilayer size by using a separator[40] or by re-forming the ruptured bilayer[41]. Since the bilayer rupture occurs stochastically, a large number of arrayed DW chambers would alternatively offer the efficient measurements. Sequential signal recordings using a multiplexer would provide an economical option to efficiently scan the large number of chambers and trace the most successful ones with a limited number of amplifiers.

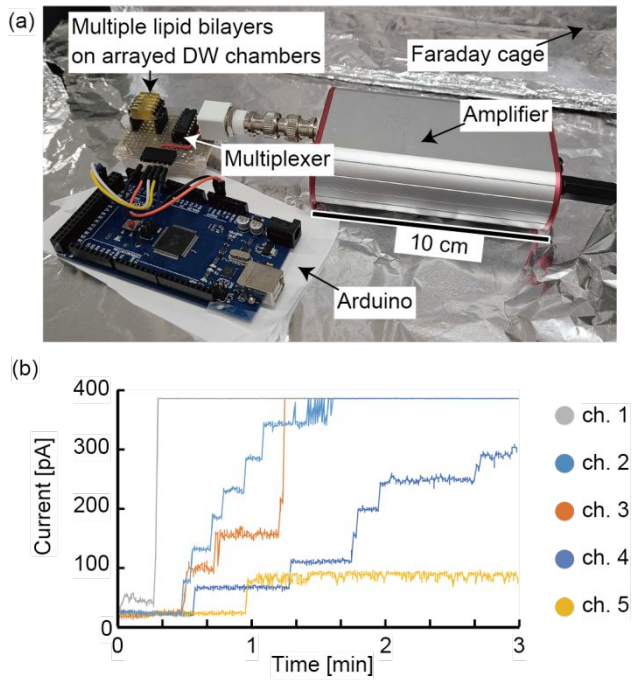

Figure 7: Simultaneous measurement of multiple lipid bilayers on the arrayed DW chambers fabricated by stereolithography. (a) Setup for simultaneous electrical recordings. (b) Representative transmembrane current signals of αHL nanopores. Applied voltage: 50 mV. Fabrication materials: microArch and Novec. Dimension: W = 80 µm, D = 600 µm, αHL concentration: 0.1 nM.

Accordingly, the stereolithographic technology, which demonstrated the reproducible, single-step fabrication of the arrayed DW chambers, would contribute to the high robustness of the lipid bilayer systems. The robustness would in turn reduce the labor cost of data acquisitions for ion channel analyses, and also pave the way for future applications of membrane proteins such as on-site chemical sensing[42].

Conclusions

We monolithically fabricated the DCM devices by using stereolithographic technology, and verified the feasibility of the devices for electrical measurements of nanopores and ion channels. High hydrophobicity and surface smoothness of the printing materials were the key factors for reproducible lipid bilayer formation on the device. With the optimized devices, the electrical noise and the rate of lipid bilayer formation were comparable to those of the devices fabricated by a conventional procedure. The extendibility of the technology was further demonstrated by the integration of microfluidic channels for solution exchangeability and the parallelization of chambers for simultaneous electrical recordings, both of which guaranteed feature designs of coming lipid bilayer devices. As the applications of membrane proteins have been expanding beyond drug discovery to chemical sensing, the technology to fabricate functionalized lipid bilayer devices with a short lead-time is becoming increasingly important. We believe the requisite characteristics of the 3D printed objects and coatings investigated in this study would be useful for the future development of the devices for practical applications of membrane proteins.

Author Contributions

Kazuto Ogishi: Conceptualization, Formal analysis, Investigation, Methodology, Validation, Writing - original draft. **Toshihisa Osaki**: Conceptualization, Funding acquisition, Methodology, Writing - review & editing. **Yuya Morimoto**: Funding acquisition, Methodology, Writing - review & editing. **Shoji Takeuchi**: Conceptualization, Funding acquisition, Methodology, Writing - review & editing, Supervision.

Conflicts of interest

S.T is an inventor on intellectual property rights related to the droplet contact method, and a stockholder of MAQsys Inc., a start-up company that applies the lipid bilayer technology based on the droplet contact method to the validation of drug candidates.

T. O is a stockholder and a board member of MAQsys Inc.

Acknowledgements

We thank Ms. Uchida (KISTEC) for the technical support. This work was partly supported by JST CREST Grant Number JPMJCR20C4 and the Program for Building Regional Innovation Ecosystem of MEXT, Japan.

References

1 R. Santos, O. Ursu, A. Gaulton, A. P. Bento, R. S. Donadi, C. G. Bologa, A. Karlsson, B. Al-Lazikani, A. Hersey, T. I. Oprea and J. P. Overington, *Nat. Rev. Drug Discov.*, 2017, **16**, 19–34.

2 T. Osaki and S. Takeuchi, *Anal. Chem.*, 2017, **89**, 19–34.

3 J. H. Lim, E. H. Oh, J. Park, S. Hong and T. H. Park, *ACS Nano*, 2015, **9**, 1699–1706.

4 H. Su, H. Y. Liu, A. M. Pappa, T. C. Hidalgo, P. Cavassin, S. Inal, R. M. Owens and S. Daniel, *ACS Appl. Mater. Interfaces*, 2019, **11**, 43799–43810.

5 R. Watanabe, N. Soga and H. Noji, *IEEE Trans. Nanotechnol.*, 2016, **15**, 70–73.

6 H. Bayley, B. Cronin, A. Heron, M. A. Holden, W. L. Hwang, R. Syeda, J. Thompson and M. Wallace, *Mol. Biosyst.*, 2008, **4**, 1191–1208.

7 K. Funakoshi, H. Suzuki and S. Takeuchi, *Anal. Chem.*, 2006, **78**, 8169–8174.

8 R. Kawano, Y. Tsuji, K. Sato, T. Osaki, K. Kamiya, M. Hirano, T. Ide, N. Miki and S. Takeuchi, *Sci. Rep.*, 2013, **3**, 1995.

9 H. Watanabe and R. Kawano, *Anal. Sci.*, 2016, **32**, 57–60.

10 M. A. Elfaramawy, S. Fujii, A. Uyeda, T. Osaki, S. Takeuchi,

Y. Kato, H. Watanabe and T. Matsuura, *Chem. Commun.*, 2018, **54**, 12226–12229.
11 T. Yamada, H. Sugiura, H. Mimura, K. Kamiya, T. Osaki and S. Takeuchi, *Sci. Adv.*, 2021, **7**, eabd2013.
12 H. Watanabe, A. Gubbiotti, M. Chinappi, N. Takai, K. Tanaka, K. Tsumoto and R. Kawano, *Anal. Chem.*, 2017, **89**, 11269–11277.
13 M. Chinappi, M. Yamaji, R. Kawano and F. Cecconi, *ACS Nano*, 2020, **14**, 15816–15828.
14 A. V. Nielsen, M. J. Beauchamp, G. P. Nordin and A. T. Woolley, *Annu. Rev. Anal. Chem.*, 2020, **13**, 45–66.
15 A. Naderi, N. Bhattacharjee and A. Folch, *Annu. Rev. Biomed. Eng.*, 2019, **21**, 325–364.
16 S. Begolo, D. V. Zhukov, D. A. Selck, L. Li and R. F. Ismagilov, *Lab Chip*, 2014, **14**, 4616–4628.
17 A. Bruin, M. S. Friddin, Y. Elani, N. J. Brooks, R. V. Law, J. M. Seddon and O. Ces, *RSC Adv.*, 2017, **7**, 47796–47800.
18 T. Ahmed, S. Driesche, J. A. Bafna, M. Oellers, R. Hemmler, K. Gall, R. Wagner, M. Winterhalter and M. J. Vellekoop, *Biomed. Microdevices*, 2020, **22**, 32.
19 N. Misawa, S. Fujii, K. Kamiya, T. Osaki, T. Takaku, Y. Takahashi and S. Takeuchi, *ACS Sensors*, 2019, **4**, 711–716.
20 E. George, P. Liacouras, F. J. Rybicki and D. Mitsouras, *RadioGraphics*, 2017, **37**, 1424–1450.
21 L. Song, M. R. Hobaugh, C. Shustak, S. Cheley, H. Bayley and J. E. Gouaux, *Science (80-.).*, 1996, **274**, 1859–1865.
22 H. Suzuki, K. V. Tabata, H. Noji and S. Takeuchi, *Langmuir*, 2006, **22**, 1937–1942.
23 R. Kawano, Y. Tsuji, K. Kamiya, T. Kodama, T. Osaki, N. Miki and S. Takeuchi, *PLoS One*, 2014, **9**, e102427.
24 O. Gülcan, K. Günaydın and A. Tamer, *Polymers (Basel).*, 2021, **13**, 2829.
25 H. Eliasova, T. Dostalova, M. Jelinek, J. Remsa, P. Bradna, A. Prochazka and M. Kloubcova, *Appl. Sci.*, 2020, **10**, 5708.
26 D. Yamaura, D. Tadaki, S. Araki, M. Yoshida, K. Arata, T. Ohori, K. Ishibashi, M. Kato, T. Ma, R. Miyata, H. Yamamoto, R. Tero, M. Sakuraba, T. Ogino, M. Niwano and A. Hirano-Iwata, *Langmuir*, 2018, **34**, 5615–5622.
27 J. W. Grate, K. J. Dehoff, M. G. Warner, J. W. Pittman, T. W. Wietsma, C. Zhang and M. Oostrom, *Langmuir*, 2012, **28**, 7182–7188.
28 H. Sugiura, T. Osaki, H. Mimura, T. Yamada and S. Takeuchi, *IEEE/RSJ Int. Conf. Intell. Robot. Syst.*, 2020, 2763–2766.
29 X. Kang, M. A. Alibakhshi and M. Wanunu, *Nano Lett.*, 2019, **19**, 9145–9153.
30 H. Ryu, A. Fuwad, S. M. Kim and T.-J. Jeon, *Colloids Surfaces B Biointerfaces*, 2021, **199**, 111552.
31 S. Kalsi, A. M. Powl, B. A. Wallace, H. Morgan and M. R. R. de Planque, *Biophys. J.*, 2014, **106**, 1650–1659.
32 R. Kawano, A. E. P. Schibel, C. Cauley and H. S. White, *Langmuir*, 2009, **25**, 1233–1237.
33 M. Mayer, J. K. Kriebel, M. T. Tosteson and G. M. Whitesides, *Biophys. J.*, 2003, **85**, 2684–2695.
34 M. Iwamoto and S. Oiki, *Sci. Rep.*, 2015, **5**, 9110.
35 W. F. Wonderlin, A. Finkel and R. J. French, *Biophys. J.*, 1990, **58**, 289–297.
36 S. Ghatta, D. Nimmagadda, X. Xu and S. T. O'Rourke, *Pharmacol. Ther.*, 2006, **110**, 103–116.
37 A. E. López-Romero, I. Hernández-Araiza, F. Torres-Quiroz, L. B. Tovar-Y-Romo, L. D. Islas and T. Rosenbaum, *Channels (Austin)*, 2019, **13**, 207–226.
38 Y. Tsuji, R. Kawano, T. Osaki, K. Kamiya, N. Miki and S. Takeuchi, *Lab Chip*, 2013, **13**, 1476–1481.
39 Y. Ito, T. Osaki, K. Kamiya, T. Yamada, N. Miki and S. Takeuchi, *Small*, 2020, **16**, 2005550.
40 A. Hirano-Iwata, K. Aoto, A. Oshima, T. Taira, R. Yamaguchi, Y. Kimura and M. Niwano, *Langmuir*, 2010, **26**, 1949–1952.
41 Y. Tsuji, R. Kawano, T. Osaki, K. Kamiya, N. Miki and S. Takeuchi, *Anal. Chem.*, 2013, **85**, 10913–10919.
42 Y. Hirata, H. Oda, T. Osaki and S. Takeuchi, *Lab Chip*, 2021, **21**, 2643–2657.